Nylon 11/Silica Nanocomposite Coatings Applied by the HVOF Process. II. Mechanical and Barrier Properties

E. PETROVICOVA,[1] R. KNIGHT,[1] L. S. SCHADLER,[2] T. E. TWARDOWSKI[1]

[1] Drexel University, Department of Materials Engineering, 3141 Chestnut Street, Philadelphia, Pennsylvania, 19104-2875

[2] Rensselaer Polytechnic Institute, Department of Materials Science and Engineering, Troy, New York 12180-3590

Received 2 August 1999; accepted 3 March 2000

ABSTRACT: Nylon 11 coatings filled with nominal 0–15 vol % of nanosized silica or carbon black were produced using the high velocity oxy-fuel combustion spray process. The scratch and sliding wear resistance, mechanical, and barrier properties of nanocomposite coatings were measured. The effect of powder initial size, filler content, filler chemistry, coating microstructure, and morphology were evaluated. Improvements of up to 35% in scratch and 67% in wear resistance were obtained for coatings with nominal 15 vol % contents of hydrophobic silica or carbon black, respectively, relative to unfilled coatings. This increase appeared to be primarily attributable to filler addition and increased matrix crystallinity. Particle surface chemistry, distribution, and dispersion also contributed to the differences in coating scratch and wear performance. Reinforcement of the polymer matrix resulted in increases of up to 205% in the glass storage modulus of nanocomposite coatings. This increase was shown to be a function of both the surface chemistry and amount of reinforcement. The storage modulus of nanocomposite coatings at temperatures above the glass transition temperature was higher than that of unfilled coatings by up to 195%, depending primarily on the particle size of the starting polymer powder. Results also showed that the water vapor transmission rate through nanoreinforced coatings decreased by up to 50% compared with pure polymer coatings. The aqueous permeability of coatings produced from smaller particle size polymers (D-30) was lower than the permeability of coatings produced from larger particles because of the lower porosities and higher densities achieved in D-30 coatings. © 2000 John Wiley & Sons, Inc. J Appl Polym Sci 78: 2272–2289, 2000

Key words: polymer nanocomposite; HVOF; thermal spray; nylon 11 coatings; wear testing

INTRODUCTION

Reinforced polymer coatings used for corrosion protection are critical in applications in which increased mechanical properties and high scratch and wear resistance are required. The properties are especially enhanced by the use of nanoscale ceramic reinforcements. Development and application of nanoreinforced polymer coatings is challenging for environmental and safety reasons because the use of volatile organic compounds and high processing temperatures must be avoided. In this work, the novel thermal spray processing of nanocomposite polymers was investigated. The results of scratch and sliding wear resistance, aqueous permeability, and dynamic mechanical analysis of thermal sprayed nanocomposite coatings are presented. The improvements in proper-

Correspondence to: T. Twardowski (tet@coe.drexel.edu).

Contract grant sponsor: National Science Foundation; contract grant number 9713650.

Journal of Applied Polymer Science, Vol. 78, 2272–2289 (2000)

ties were related to the filler content, filler surface chemistry, filler/matrix interactions, coating microstructure, and polymer crystallinity.

Relevant theoretical models for the prediction of nanocomposite properties including modulus, damping, and permeability are introduced. The calculated predictions are compared with experimental results and the results used to elucidate possible reinforcing mechanisms in the sprayed nanocomposite coatings.

BACKGROUND

The inclusion of nanoparticulates in thermoplastics has been shown to result in substantial changes in polymer properties, even compared with the effects of adding micron-sized reinforcements.[1–9] Sumita et al.[1] demonstrated that 7-nm silica reinforcements in semicrystalline nylon 6 increased the yield stress by 30% and Young's modulus by 170% compared with pure polymers, whereas micron-sized reinforcements decreased the yield stress and only marginally increased the modulus. They observed similar effects for nanosized fillers in polypropylene where the dynamic storage modulus increased by 100% with the addition of 20 wt % of 7-nm silica particles whereas the addition of the same amount of 200-μm glass particles caused only a marginal increase in the dynamic storage modulus.[2] The improvement in properties of layered nanocomposites was even more pronounced because of the high aspect ratio of the fillers. The dynamic storage modulus of a nanocomposite containing as low as 4 vol % of mica-type silicate in an epoxy matrix increased by 58% in the region below the glass transition temperature (T_g) and by 450% in the rubbery region.[3] Permeability of water in poly(ϵ-caprolactone) also decreased by an order of magnitude with the addition of 4.8 vol % of mica-type silicate.[4] A 60% decrease in permeability in polyimide composites containing as little as 2% mica was reported, whereas the thermal expansion coefficient was reduced by 25%.[5]

The achievement of a homogeneous distribution of nanosized fillers represents an important technical challenge in their processing because decreasing filler particle size causes a significant increase in melt viscosity.[6] Large amounts of solvent (20 to 60 vol %)[7] or higher mixing temperatures were used during processing of particulate filled nanocomposites.[1,2] The methods currently used to produce layered nanocomposites are intercalation (inserting) of the polymer between the host silicate layers or delamination of the silicate layers and dispersing them within a polymer matrix for which the intercalating monomer or polymer was also dissolved in the solvent. Other methods include *in situ* polymerization, and sol-gel processing for polyamide-silica nanocomposites.[8] Recently, some progress in melt processing of mica-type nanocomposites has been reported.[9]

An excellent solution to the processing limitations of polymer/ceramic nanocomposites, such as the use of solvents, is thermal spraying. During a thermal spray process, polymer particles are heated in a thermal jet (created either by a plasma or via combustion), and then accelerated toward the substrate. The polymer viscosity is reduced in-flight by heating and melting, and the particles "splat" against the substrate. This environmentally compliant coating application technique does not require solvents because the starting material is in the form of a powder. Other important advantages of thermal spraying over other coating processes (such as sol-gel, fluidized bed, or vapor deposition processes) are that the deposition of nanoreinforced composites is not limited by the size of the part to be coated, and that the coatings can be readily applied in the field. One of the most important applications for thermally sprayed coatings is their use as corrosion protection coatings for metallic substrates. Previous results[10] demonstrated that the high velocity oxy-fuel (HVOF) combustion spray technique is also a viable method for the processing of nanoreinforced polymers.

The processing, physical properties, and microstructures of thermally sprayed silica or carbon black/nylon11 nanocomposite coatings have already been evaluated as a function of processing conditions and discussed in a previous publication.[11] It was demonstrated that combusting gas mixtures with a low hydrogen content were needed for optimal jet temperature, resulting in better particle flow and improved filler distribution in the polymer matrix. Thermally sprayed nanocomposite coatings exhibited an increase in crystallinity relative to unfilled coatings because of the presence of the filler: up to a 15% and up to a 9% increase in coatings produced from 60 μm and 30 μm polymer particles, respectively, relative to nonreinforced thermally sprayed polymer. Coatings produced from smaller polymer particles also had higher densities and lower porosity.

THEORY

Extensive development of theories explaining reinforcement mechanisms and for the prediction of the properties of reinforced composites abound.[12–34] Application of these to nanocomposite properties due to the addition of nanofillers is not yet as well established.

A very general approximation of the behavior of filled polymers is the rule of mixtures, which provides upper and lower boundaries to mechanical response. The upper bound eq. (1) reflects strong adhesion between the polymer and filler and a high filler aspect ratio, whereas the lower bound eq. (2) is more applicable to rigid spherical particles:

$$M_c = M_p\phi_p + M_f\phi_f \tag{1}$$

$$M_c = \frac{M_pM_f}{M_p\phi_f + M_f\phi_p} \tag{2}$$

where M_c is the modulus (shear, elastic, or bulk) of the composite, M_p and M_f are the moduli of the polymer matrix and filler, and ϕ_p and ϕ_f are the volume fractions of the polymer and filler, respectively. The moduli of most particulate filled polymers have been shown to lie somewhere between these two limits.[12] The main reinforcing mechanism was assumed to be the effectiveness of load transfer from the particles to the polymer matrix.

Particle geometry, size, degree of dispersion and agglomeration, and interfacial interactions strongly affect the final properties of filled polymers. Simple theoretical models describing the reinforcement of a material, such as the one proposed by Einstein[13] and later extended by Guth and Smallwood,[14] assumed perfect interfacial adhesion. These are valid up to low filler volume fractions, because they ignore any mechanical interaction between neighboring particles. A relation that also accounts for the effect of adhesion efficiency between the two phases has been suggested by Sato and Furukawa.[15] The models proposed by Mooney,[16] Eilers and van Dyck,[17] and Bills et al.[18] took into consideration a number of effects from the filler distribution. Experimental deviations from the theoretical predictions of these models due to particle size were, however, reported.[19] Quemada[20] introduced a variable coefficient to account for inter-particle interactions and differences in particle geometry. Frankle and Acrivos[21] introduced the concept of maximum packing fraction to account for differences in particle geometry.

Kerner's equation[22] was derived to calculate the modulus of a composite containing nearly spherical particles with some adhesion between the phases at up to moderate concentrations. Nielsen's modification of Kerner's equation was more versatile at low reinforcement concentrations, taking into account both the maximum packing fraction of the filler, inter-particle interactions and the relative modulus of the two constituents[23]:

$$\frac{M_c'}{M_p} = \frac{1 + AB\phi_f}{1 - \psi B\phi_f} \tag{3}$$

where A accounts for the contribution of polymer–filler interactions and factors such as the geometry of the filler phase. A is determined by the generalized Einstein coefficient k_E (tabulated in ref. 12) from:

$$A = k_E - 1 \tag{4}$$

ψ in eq. 3 is a reduced concentration term dependent on the maximum packing fraction ϕ_m of the filler in the polymer (also tabulated in ref.[12]):

$$\psi = 1 + [(1 - \phi_m)/\phi_m^2]\phi_f \tag{5}$$

The constant B takes into account the relative moduli of the filler and the matrix; its value is 1.0 for very large M_f/M_p ratios. It is defined as:

$$B = \frac{M_f/M_p - 1}{M_f/M_p + A} \tag{6}$$

The principle of viscoelastic correspondence permits the substitution of storage or complex moduli into eq. (3). The Einstein coefficient k_E for dispersed spheres with perfect adhesion to a matrix, estimated by Lewis and Nielsen,[24] has a value of 2.5. The value drops to 1.0 if there is perfect slippage at the interface. For large-scale agglomeration, or in the case of elongated particles, the Einstein coefficient and the value of A are expected to be higher (>3) than for well dispersed spherical particles.[12]

Filler size effects were not directly considered in traditional reinforcement models. As shown by Boluk and Schreiber,[25] however, experimentally measured moduli of nanofilled polymers closely fit

those calculated according to the Nielsen model. The modulus of thermally sprayed coatings will be calculated using this model.

The modulus of polymers also increases rapidly with crystallinity, especially above T_g. Crystallites are expected to act as crosslinks by tying segments of many molecules together. Furthermore, crystalline regions have higher moduli than amorphous ones, and as a result can behave as rigid filler in an amorphous matrix. To a first approximation, the modulus above T_g is related to the degree of crystallinity, expressed as a weight fraction w_c, by eq. (7) proposed by Nielsen and Landel[12]:

$$\log_{10}G \cong 5.763 + 4.77w_c \tag{7}$$

The comparison of the predicted modulus based on the amount of crystallinity with the experimental data can therefore be used to elucidate one of the possible reinforcing mechanisms.

Mechanical damping is also affected by the presence of fillers and by filler/matrix interface conditions. Damping behavior is particularly interesting around the T_g because of the changes occurring there due to the filler. As shown by Nielsen,[23] in filled polymers damping behavior is related to the polymer volume fraction:

$$\tan \delta_c = \tan \delta_p(1 - \phi_f) \tag{8}$$

where ϕ_f is the volume fraction of the filler, and $\tan \delta_c$ and $\tan \delta_p$ are the loss moduli of the composite and polymer, respectively. This equation is valid for composites filled with nonagglomerated rigid solid particles and without interactions.

Significant physicochemical interactions or bonds between the polymer and the filler can contribute to the formation of an interface with distinctive behavior,[26] induce crystallization or orientation of the chains in the immediate vicinity of the filler surface,[27] or result in the formation of a "bound" or immobile polymer layer.[28] According to Boluk and Schreiber,[25] eq. (8) can be rewritten, with the introduction of a correction parameter B, as originally suggested by Iisaka and Shibayama[29]:

$$\tan \delta_c = \tan \delta_p(1 - B\phi_f) \tag{9}$$

The correction parameter B is related to the effective thickness of the particle–matrix interface layer through:

$$B = (1 + \Delta R/R)^3 \tag{10}$$

where R is the mean radius of the dispersed particles, and ΔR is the thickness of the immobilized layer. This hypothetical boundary layer in the presence of a filler is considered, by several authors, to be another possible reinforcing mechanism beyond the traditional load transfer, especially in nanocomposites where the reinforcing effect of the filler is unusually large even at low filler contents.[25–29] Predictions calculated according to this model will be used for comparison with results of this work.

One strong indicator of the corrosion resistance of a coating is its resistance to water permeation. Predictions of permeation processes in heterogeneous systems are as complex as the mechanical responses; the overall transport depends on the amount, distribution and nature of the components, the magnitude of component interactions, and any interfacial phenomena. Permeation through a polymer is governed by two intrinsic factors: polymer chain segment mobility and defect structures, such as micro-cracks, pores, and variations in density.[30] The presence of regions which are inaccessible to the diffusing species within a polymer effectively increase the diffusion path length and tortuosity and reduce its permeability. A further decrease in diffusion coefficient has been observed with increasing crystallinity by the same process.[31,32] In the case of plate or flake-shaped particles diffusion depends strongly on their orientation.[33] The permeability of polymers filled with flaky or lamellar particles is usually lower than those filled with spherical fillers.[34]

The quantification of changes in the permeation resistance associated with the heterogeneities in a continuous polymer medium is not straightforward, but some simplified approaches have been developed. Permeability of polymers containing an impermeable phase such as fillers or impermeable polymer crystals in the absence of porosity can be estimated from the model proposed by Barrer[35]:

$$P_i = P_0(1 - \nu_i)^2 \tag{11}$$

where P_i is the permeability of polymer containing an impermeable phase, P_0 is the permeability of an amorphous or unfilled polymer, and υ_i is the volume fraction of the impermeable phase. This model is used to predict permeability for nanocomposite coatings in this work and the results are compared with the experimental data.

Table I Nominal Vs. Actual Filler Contents in Composite Powders and Filled Nylon 11 D-30 and D-60 Coatings

Nominal Filler Content in Powder (vol %)	Silica in D-60 Coatings (vol %)	Silanated Silica in D-60 Coatings (vol %)	Silica in D-30 Coatings (vol %)	Carbon Black in D-60 Coatings (vol %)
5	2.4	3.2	—	4.9
10	4.5	6.2	4.6	7.1
15	6.7	7.7	6.9	10.3
20	6.9	—	—	10.1

EXPERIMENTAL

Materials

Nylon 11 ("French Natural ES," Elfatochem North America, Inc., King of Prussia, PA) was chosen as the matrix material because it has a high chemical resistance and wide processing window–large difference between the melting (~183°C) and degradation temperatures (~360–550°C). The T_g is typically 53°C, varying slightly as a function of reinforcement and crystallinity. Nylon 11 has been widely used as a coating because of an excellent combination of properties, such as low-temperature flexibility, low coefficients of friction, superior mechanical strength, and high chemical resistance. In this study, nylon 11 powders with mean particle sizes of 30 and 60 μm, designated as D-30 and D-60, respectively, were used.

Silica powders, 7 and 12 nm ("R 812" and "A 200," from Degussa Corporation, Ridgefield Park, NJ), with hydrophobic and hydrophilic surface chemistries, respectively, 5 μm precipitated silica, 6 nm carbon black (Degussa Corporation) and A 1100 gamma-aminopropyltriethoxy silane modified silica, referred to as "silanated silica," were used for nylon 11 reinforcement to determine the effect of the different surface chemistries and powder sizes on the nanocomposite properties. Silanes were applied to decrease or remove any hydrophilic properties of the silica surface, to reduce agglomeration, and to incorporate new organofunctional groups with higher chemical affinity to specific polymers on the SiO_2 surface.[36] Silica was mixed for 3 h in a silane-toluene solution at 5 wt % of silica in toluene and then dried at a temperature 105°C to remove the solvent. Coatings with nominal 10 vol % of precipitated silica with a mean particle size of 5 μm were also produced to show the effect of particle size on the coating properties.

Co-spraying two different powders can result in significant segregation in the jet, because of differences in powder size and density. A composite powder, containing both materials in a single powder, aids both in simultaneous powder feeding into the HVOF spray jet and in distribution of the filler in the coating. Nylon 11 powder was dry ball-milled together with the nanoparticulate phase for 48 h in a Norton Ball Mill using zirconia balls to create the composite powder.

The nominal content of filler in the powder compositions sprayed ranged from 5 to 15 vol %. Table I shows the actual filler content in the nanocomposite coatings, determined by thermogravimetric analysis as described below. In the discussion of the results, except where noted, specimens are labeled according to the nominal volume percent of filler in the starting materials.

Coating Procedure

A Stellite Coatings' Jet Kote II® HVOF combustion spray gun with internal powder injection and a 0.076 m (3″) long and 0.008 m (5/16″) diameter nozzle, was used to spray the composite powders. Typical processing parameters, detailed in a previous publication,[11] are listed in Table II.

The nanosized silica-reinforced nylon 11 composites were deposited onto 25.4 × 75.2 × 3 mm (1″ × 3″ × 0.125″) aluminum (6061) substrates and also 60 mm diameter aluminum (6061) discs. Before spraying, the substrates were grit-blasted using 1600 μm SiC grit and cleaned in an ultrasonic ethanol bath. Substrates to be used to support coatings for subsequent thermal and structural analyses were polished instead of grit-blasted to allow for easy removal of the coating.

The substrates were preheated to approximately 80°C by traversing the HVOF jet over the substrate surface before powder injection. Typical coating thicknesses ranged between 250 to 350 μm (0.01–0.014 in.).

Table II HVOF Processing Parameters Used for Spraying of Polymer Nanocomposite Coatings

Parameter	SI Units	Standard[a] Units
Total gas flow rate	14.9–17.0 $\times 10^{-3}$ m^3 s^{-1}	1600–1820 scfh
Hydrogen/oxygen ratio	0.29–0.50	—
Hydrogen/oxygen gas pressure	0.83 MPa	120 psi
Powder feed rate	0.25 g s^{-1}	15 g min^{-1}
Powder carrier gas	Nitrogen	—
Powder carrier gas flow rate	0.5 $\times 10^{-4}$ m^3 s^{-1}	60 scfh
Powder carrier gas pressure	0.97 MPa	140 psi
Sample velocity	Stationary	—
Gun horizontal surface speed	0.23 m s^{-1}	45 ft. min^{-1}
Step size per pass	3.2 $\times 10^{-3}$ m	0.126 in.
Spray distance	0.2 m	8 in.

[a] Traditional thermal spray industry standard units.

Coating Characterization

The "as-sprayed" coatings exhibited peak-to-valley roughnesses up to 30 μm and therefore before scratch and wear testing the coating surfaces were polished using SiC paper to a roughness of <6 μm.

Scratch tests were performed using a BYK Gardner SG-8101 balance beam scrape adhesion and mar tester according to ASTM D 5178-91[37] at applied loads of 2, 2.5 and 3 kg. Scratch profiles and scratch depths were measured using a Hommelwerke model Dektak II stylus tracing profilometer. A typical scratch profile is shown in Figure 1. Scratch results represent the mean of nine measurements performed on three different specimens.

Sliding pin-on-disk wear tests were conducted using an AMTI Model C tribometer, according to ASTM G 99-90, using a 10 mm diameter 52100 stainless steel ball as a counterbody. The coatings were tested at room temperature in ambient air for 15,000 cycles, with a 10N applied load, at a surface sliding speed of 0.68 m s^{-1}. Wear track cross sectional areas were measured using the Hommelwerke profilometer. The track profile was measured at four points (Figure 2) on two wear discs with the same type of coating. Results were the mean of eight measurements.

The coefficient of friction μ was calculated from the wear data using:

$$\mu = \frac{F}{L} \tag{12}$$

where F is the friction force (N) and L the normal load (N). The data represent mean coefficient of friction under steady-state wear conditions.

Dynamic mechanical analysis was performed using a Rheometrics Scientific ARES analyzer operated in torsion mode. The in-phase and out-of-phase responses were measured at a frequency of 1 Hz over a temperature range of 20 to 150°C on 5-mm-wide strips of coatings.

The permeability of thermally sprayed coatings was measured using the permeability cup method (ASTM D1653-93[38]) according to Test Method A, under Condition A (Figure 3) at 50% relative humidity and at 23°C over a 21-day period. Under steady state conditions, the increase in weight with time corresponded to the amount

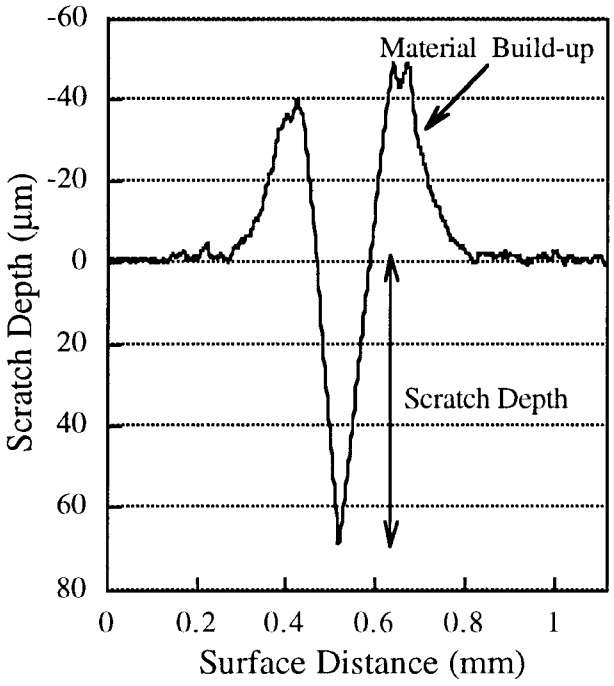

Figure 1 Typical scratch profile.

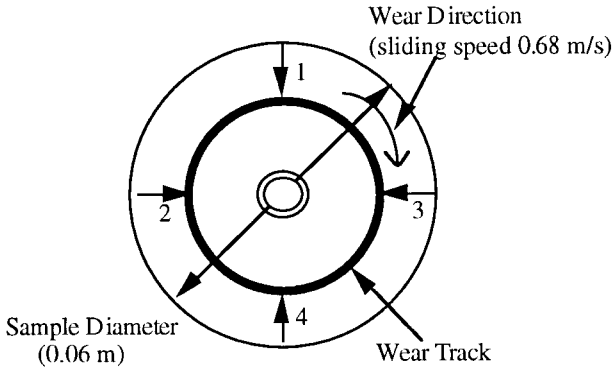

Figure 2 Locations of the wear track and profile measurements.

of water vapor diffusion. At least three testing cycles were performed for each coating composition.

Standard deviations are shown as error bars for the data obtained from averaging statistically significant numbers of measurements (at least five); otherwise a data range is reported.

RESULTS AND DISCUSSION

Scratch Resistance

Scratch resistances of 15% D-60 sprayed coatings at 2-kg applied load are shown in Figure 4. With an increase in reinforcement content the scratch depth of all composite coatings decreased. A maximum scratch resistance was achieved for coatings of either 15% hydrophobic silica or carbon black particles in a nylon 11 D-60 matrix at an applied load of 2 kg (Fig. 4). These increases represented 35 and 30% improvements in scratch resistance of nanocomposite coatings over pure nylon 11 D-60 coatings, respectively.

Scratch depth increased with increasing applied load for all samples (Fig. 4) but an increase

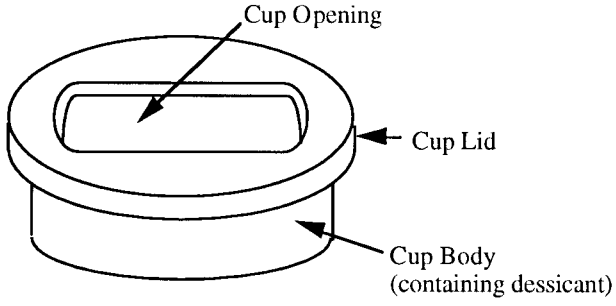

Figure 3 Permeability testing cup assembly.

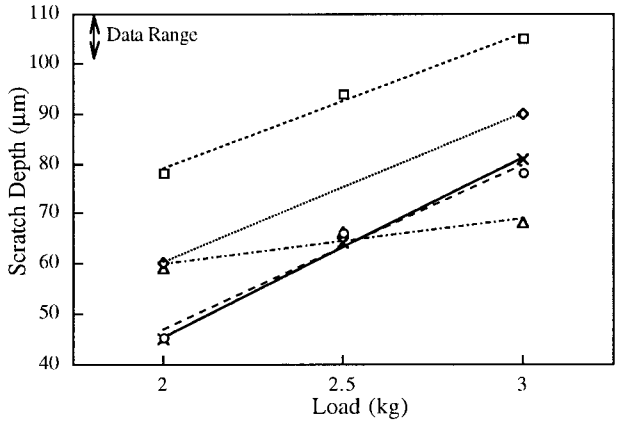

Figure 4 Scratch depth of thermally sprayed nylon 11 D-60 coatings containing: (□) 0, and nominal 15 vol % of: (○) hydrophobic silica, (◇) hydrophilic silica, (△) silanated silica, and (×) carbon black fillers.

in reinforcement similarly decreased the scratch depth. Fifteen percent silanated silica nanocomposites exhibited the lowest scratch depths of all samples at 3 kg load, a 35% decrease relative to pure thermally sprayed nylon 11 D-60. Silanated silica filled coatings also did not exhibit as great an increase in scratch depth with load as the untreated silica coatings. A more even dispersion of the reinforcing particles in the silanated samples[11] was likely the cause of this behavior.

The scratch depths of D-60 coatings reinforced with micron-sized particles applied by the fluidized bed process were measured to be 57, 60, and 63 μm at 2, 2.5, and 3 kg loads, respectively. These were comparable to thermally sprayed reinforced D-60 coatings.

The scratch depth of the D-30 thermally sprayed composite coatings decreased slightly with increasing reinforcement content relative to pure D-30 coatings (Fig. 5). This decrease was not as pronounced, however, as in the case of the D-60 composite coatings (Fig. 6). The differences in scratch depth were closely related to the coating microstructure and polymer crystallinity (Fig. 7). The crystallinity content dominated the scratch resistance at lower loads (2 and 2.5 kg). This result was consistent with known improvements in hardness and mechanical properties of polymers such as elastic modulus and yield stress with increasing crystallinity.[39,40] Figures 6 and 7 show that particle/matrix interfacial interactions had a significant effect on both the scratch behavior and the degree of crystallinity in the D-60 nanocomposite coatings. Figures 6 and 7 also

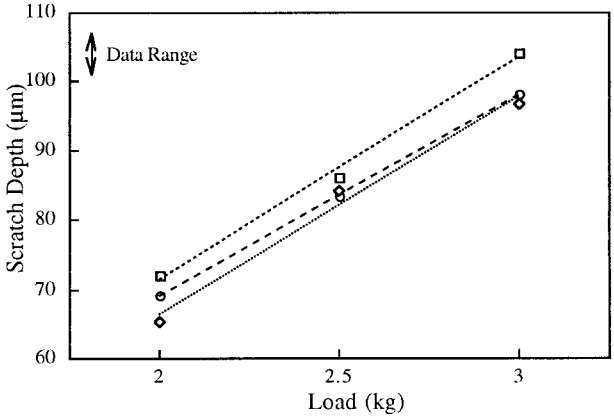

Figure 5 Scratch depth of thermally sprayed nylon 11 D-30 coatings containing: (□) 0, and nominal 15 vol % of: (○) hydrophobic silica and (◇) hydrophilic silica fillers.

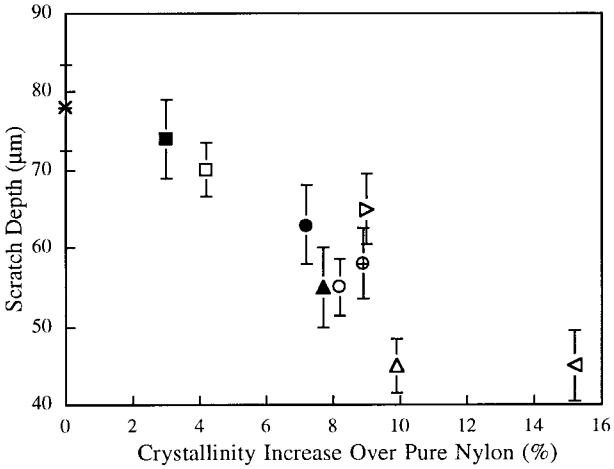

Figure 7 Scratch depth of thermally sprayed nylon 11 D-60 coatings as a function of filler and crystallinity content. The symbols represent: (□, ○, △) hydrophobic silica; (■, ●, ▲) hydrophilic silica; (▷) silane treated silica; (⊕, ◁) carbon black. The star, square, circle, and triangle symbols represent 0, 5, 10, 15 vol % nominal filler contents, respectively.

show that 15% hydrophobic silica and 15% carbon black reinforced composites both exhibited identical scratch resistances, despite large differences in crystallinity.

The improvement in scratch resistance for the D-30 coatings as a function of crystallinity is shown in Figure 8. A comparison of Figures 7 and 8 indicated a greater increase in crystalline content in the D-60 coatings than in the D-30 composite coatings.

It was hypothesized that efficient load transfer was further affected by the degree of particle/matrix interactions. These interactions depend on various factors, including the chemistry of the reinforcement surface, the efficiency of coupling between the particle and the matrix, and on the reinforcement dispersion. In Figure 9(a,b), typical scratch microstructures are shown. Figure 9(a) shows a scratch in an unreinforced D-60 coating where shearing of the polymer matrix along the whole length of the scratch is clearly visible. Numerous sheared, torn, and uneven surfaces appeared as white marks in the scratch valley. In a reinforced coating, as shown in Figure 9(b), shearing was greatly reduced. Damage to the matrix appeared to be localized to the polymer-rich areas

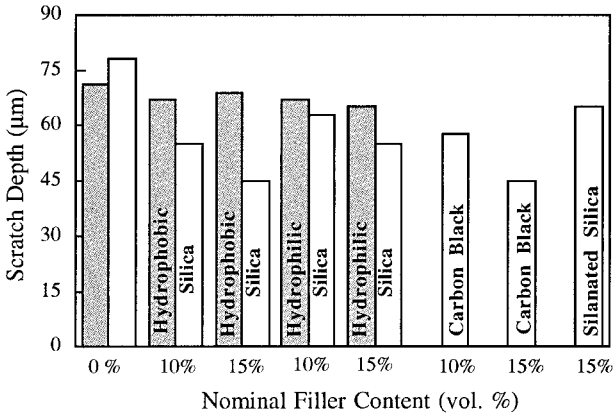

Figure 6 Scratch depth of thermally sprayed coatings as a function of filler type and content at 2-kg load. Gray and white bars represent D-30 and D-60 nylon 11 matrices, respectively.

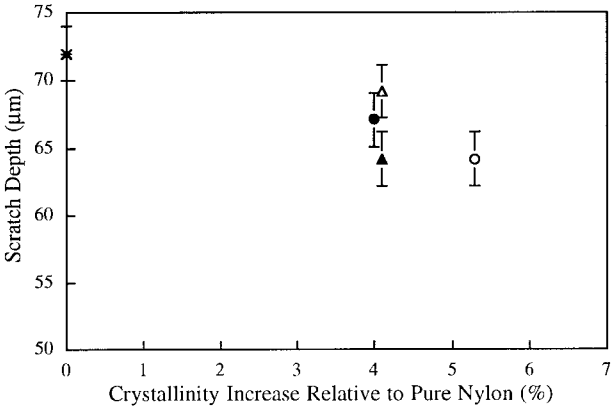

Figure 8 Scratch depth as a function of filler and crystallinity content for D-30 coatings. Legend: (✳) 0, (○) 10, (△) 15 vol % of hydrophobic silica, and (●) 10, (▲) 15 vol % of hydrophilic silica nominal contents.

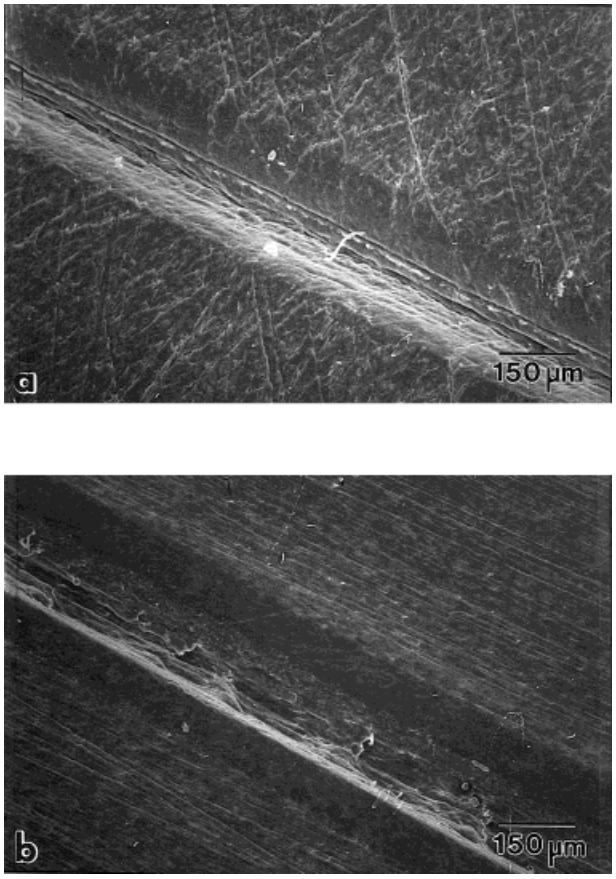

Figure 9 SEM micrographs of scratch surfaces of (a) an unfilled D-60 thermally sprayed nylon 11 coating, (b) a nylon 11 D-60 coating with nominal 10 vol % hydrophobic silica content.

inside "the cell" (as described previously[11]), seen as repeating valleys along the scratch. Only a few sheared layers appeared to have been separated from the polymer matrix. The reinforced areas, consisting of embedded particles on the polymer particle surface, exhibited greater resistance to scratch penetration and material damage than nonreinforced areas. In the case of nonreinforced coatings, the scratch valley was more acute and deeper than that of reinforced coatings.

Results indicated that filler content and crystallinity had a dominant effect on scratch resistance, with an additional dependence on reinforcement distribution and chemistry.

Sliding Wear Resistance

Figure 10 shows the effect of reinforcement on the wear resistance of D-60 coatings. Wear decreased rapidly for all types of coatings with inclusion of the reinforcement. The largest improvement, 48 and 67% wear track area reductions, occurred for 15% hydrophobic silica and 15% carbon black coatings, respectively. Large differences in wear performance were found for different types of particles and between samples with different crystallinity and filler contents, similar to the behavior described for scratch resistance. The wear resistance of a thermally sprayed nylon 11 coating reinforced with a nominal 10 vol % of 5-μm particle size precipitated silica is included for comparison. As shown in Figure 10, this exhibited a 13% wear track area reduction, but the reinforcement was significantly less effective than any of the nanoreinforcements at an equivalent load.

The results in Figure 11 show again that coatings with the highest filler and crystallinity contents, 15% hydrophobic silica and 15% carbon black composites, exhibited the highest wear resistance. In the case of 15% hydrophobic silica, a 48% decrease in wear track area was measured. The largest improvement in wear performance, a 67% decrease in wear track area, was measured for 15% carbon black filled coatings. The results for wear performance were consistent with scratch resistance results.

Figure 12(a,b) shows micrographs of typical wear tracks for pure and reinforced D-60 coatings. The wear surfaces showed wear sheet formation and delamination in the sliding direction. The damage in the wear tracks of reinforced coatings was significantly reduced [Fig. 12(b)], although the wear mechanism appeared to be the

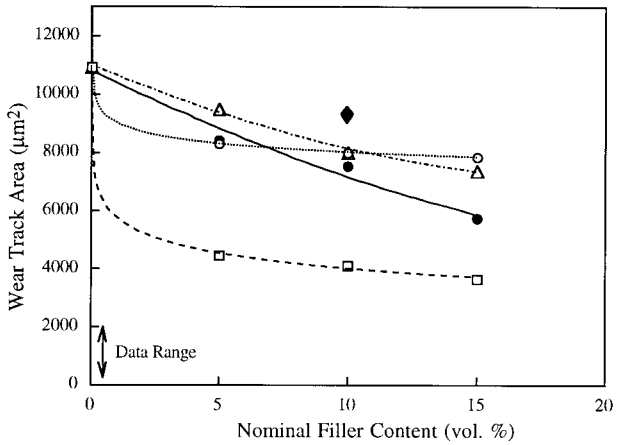

Figure 10 Wear track area of thermally sprayed nylon 11 D-60 coatings as a function of filler content. Symbols represent: (○) hydrophilic silica, (●) hydrophobic silica, (△) silanated silica, (♦) 5 μm precipitated silica, and (□) carbon black fillers.

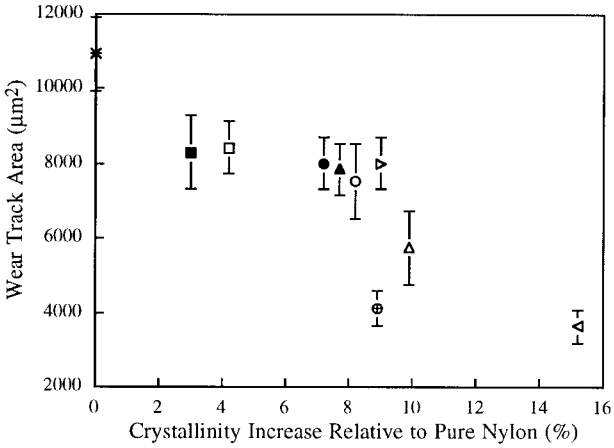

Figure 11 Wear track area of D-60 nanocomposite coatings as a function of filler and crystallinity content. Symbols represent: (□, ○, △) hydrophobic silica, (■, ●, ▲) hydrophilic silica, (▷) silane treated silica, (⊕, ◁) carbon black. 0, 5, 10, and 15 vol % nominal filler contents are represented by star, square, circle, and triangle symbols, respectively.

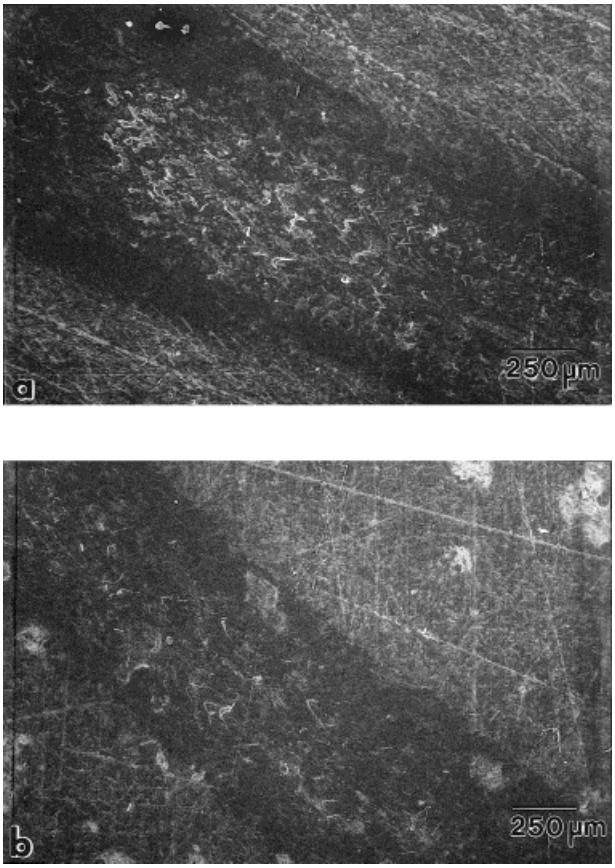

Figure 12 SEM micrographs of wear track surfaces of (a) an unfilled thermally sprayed nylon 11 D-60 coating, (b) a nylon 11 D-60 coating with nominal 10 vol % hydrophobic silica content.

same as for the pure polymer coatings. No wear craters were observed in the wear-damaged area, which would be characteristic of particle pull-out. The greater wear track area reduction in carbon black reinforced coatings may also have been due to the so-called "self-lubricating" nature of the carbon black particles.[41]

The results of wear testing of D-30 coatings are shown in Figure 13. The wear track area of these thermally sprayed nanocomposite coatings decreased with the addition of reinforcement by up to 25% relative to pure D-30 polymer coatings. The largest reduction in wear track area was observed for 10% hydrophobic silica filled coatings. D-30 coatings exhibited lower wear resistance than equivalent D-60 coatings, similar to the behavior observed for scratch resistance. Again, this was most probably due to the lower crystallinity contents of the D-30 coatings.

Coefficients of friction (μ) of the sprayed coatings are summarized in Table III. The coefficients of friction of D-60 reinforced coatings increased slightly with the addition of reinforcement relative to the pure nylon D-60, whereas the coefficient of friction of the D-30 nanocomposite coatings remained nominally the same as that of the pure D-30 polymer coatings. An increasing μ with increasing reinforcement content was also reported for high density polyethylene filled with silica gel.[42] Ramasubramanian et al.[42] reported an initial increase in μ, followed by a decrease for

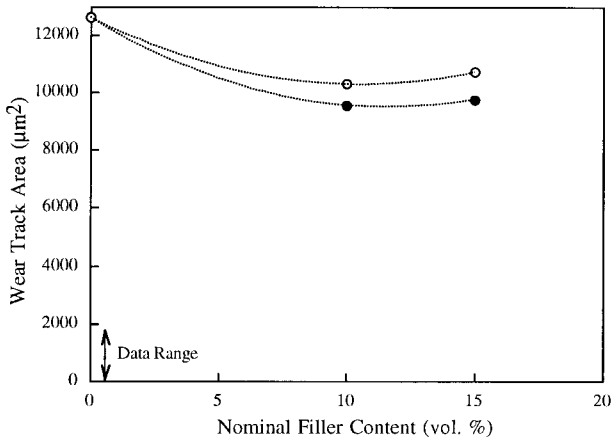

Figure 13 Wear track area of nylon 11 D-30 coatings as a function of filler content. Symbols represent: (○) hydrophilic silica and (●) hydrophobic silica fillers.

Table III Coefficients of Friction of Thermally Sprayed Nanocomposite Coatings

Silica Content (Nominal Vol %)	Silica Surface Chemistry	Nylon 11 Matrix	Mean Coefficient of Friction
0	—	D-60	0.24
0	—	D-30	0.29
5	Hydrophobic	D-60	0.24
5	Hydrophilic	D-60	0.27
5	Silanated	D-60	0.25
10	Hydrophobic	D-60	0.28
10	Hydrophilic	D-60	0.25
10	Silanated (5 μm)	D-60	n/a
10	Precipitated	D-60	0.33
10	Hydrophobic	D-30	0.29
10	Hydrophilic	D-30	0.28
15	Hydrophobic	D-60	0.30
15	Hydrophilic	D-60	0.29
15	Silanated	D-60	0.25
15	Hydrophobic	D-30	0.28
15	Hydrophilic	D-30	0.28

graphite and molybdenum disulfide filled polyethylene at higher filler contents. This critical content seemed to be dependent on the type of filler used and the testing conditions. Clerico[43] reported that the coefficient of friction decreased only when a polymer transfer layer was formed on the metal counterbody, thus changing the contact conditions. The addition of a larger size filler resulted in a larger increase in μ than was observed for nanoreinforcement, as is more typically expected from filled coatings.[42,43]

Dynamic Mechanical Properties

A series of representative storage modulus (G') curves as a function of temperature, recorded at 1 Hz for both D-30 and D-60 coatings containing 0–15% of silica are shown in Figure 14(a) and (b), respectively. The storage moduli both below and above the T_g increased with increasing amounts of silica reinforcement. The curves for the D-30 coatings [Fig. 14(a)] clearly show the region associated with the T_g. A clear transition was also observed for D-60 coatings [Fig. 14(b)]. In the case of D-60 reinforced coatings, with a 120% higher modulus than pure polymer coatings, the glassy plateau and smaller decrease in slope of the G' curve relative to D-30 coatings indicated a higher crystallinity content in the D-60 coatings (also confirmed by differential scanning calorimetry and X-ray analysis[11]). For both the D-30 and D-60 matrices, hydrophobic silica reinforced coatings exhibited larger increases in dynamic storage modulus than coatings with the same content of hydrophilic silica.

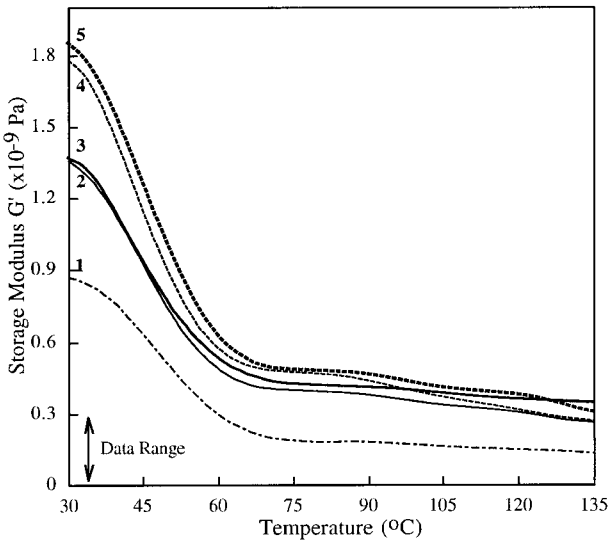

(a)

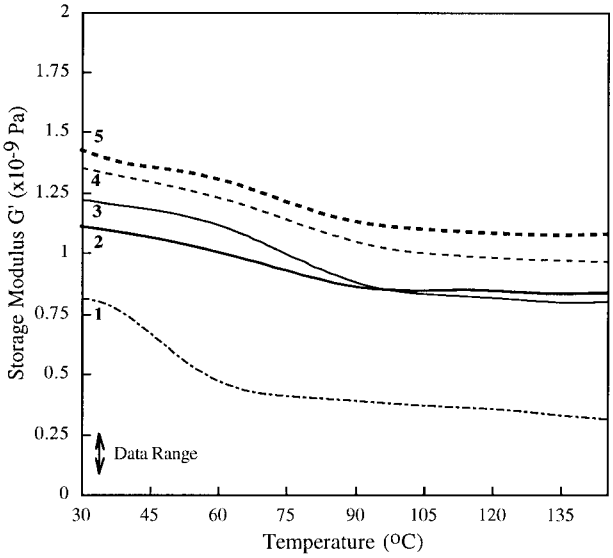

(b)

Figure 14 (a) Temperature dependence of the storage modulus G' of thermally sprayed D-30 nylon 11 coatings. Lines represent: (1) 0, (2) nominal 10, and (4) 15 vol % of hydrophilic silica; (3) nominal 10 and (5) 15 vol % of hydrophobic silica. (b) Temperature dependence of the storage modulus G' of thermally sprayed D-60 nylon 11 coatings. Lines represent: (1) 0, (3) 5, and (4) 15 vol % of hydrophilic silica; (2) 10 and (5) 15 vol % of hydrophobic silica nominal content.

Table IV Dynamic Storage Modulus G' of Thermally Sprayed Nanocomposite Coatings

Silica Content (Nominal Vol %)	Silica Surface/Filler Type	Polymer Matrix	G' at 30°C (GPa)	G' at 70°C (GPa)
0	—	D-60	0.65	0.36
0	—	D-30	0.86	0.35
5	Hydrophobic	D-60	1.15	0.86
5	Hydrophilic	D-60	1.58	1.07
5	Silanated	D-60	1.25	0.39
5	Carbon black	D-60	0.48	0.29
10	Hydrophobic	D-60	1.10	0.89
10	Hydrophobic	D-30	1.38	0.59
10	Hydrophilic	D-30	1.38	0.54
10	Silanated	D-60	1.29	0.61
10	Carbon black	D-60	0.50	0.32
15	Hydrophobic	D-60	1.39	1.06
15	Hydrophobic	D-30	1.83	0.61
15	Hydrophilic	D-60	1.31	0.99
15	Hydrophilic	D-30	1.79	0.56
15	Silanated	D-60	1.98	0.83
15	Carbon black	D-60	0.50	0.25

The dynamic storage moduli of thermally sprayed coatings at 30 and 70°C are summarized in Table IV. The largest increase, 205%, in the glass storage modulus was observed for the 15% silanated silica filled D-60 coatings, believed to be due to the improved particle distribution in the polymer matrix, in addition to the increase due to crystallinity. The glass storage modulus of D-60 coatings at 30°C increased by 120% and 100% relative to pure nylon 11 D-60 for hydrophobic and hydrophilic silica, respectively. The glass storage modulus of D-30 coatings at 30°C increased by 182% and 175% for hydrophobic and hydrophilic silica, respectively, relative to pure nylon 11 D-30 coatings. The glass storage moduli of D-30 coatings were typically higher, in the range 0.86–1.83 GPa, relative to the D-60 coatings, with moduli ranging between 0.65–1.39 GPa. This was believed to be the result of the improved filler distribution in the D-30 coatings and more efficient load transfer between the polymer matrix and the reinforcing particles.

The opposite trend was observed for the storage modulus at 70°C. Both D-30 and D-60 reinforced coatings exhibited significantly higher moduli compared with coatings of the corresponding pure polymer matrix. In the case of D-30, the dynamic storage modulus was up to 70% higher, and in the case of D-60 an increase of up to 195% relative to pure polymer coatings was observed. This was believed to be due to higher crystallinity contents in the D-60 coatings.

Predictions of the nanocomposite moduli, calculated according to eqs. (1), (2), and (3), are shown in Figures 15(a) and (b) together with experimental values as a function of the reinforcement content. All the composite coatings exhibited a modulus higher than that calculated by the lower bound prediction (lines numbered 1). This may be due to particle/matrix and particle/particle interactions or variations in crystallinity. The solid lines 2, 3, and 4 were generated for A ranging between 2 and 4.5 with a maximum packing fraction $\phi_m = 0.37$, assuming a random close packing of agglomerated filler. The data for the D-30 silica reinforced coatings closely fit calculations for $A = 3$. For silica filled D-60 coatings the fit was closer for values of A between 3 and 4. There was a large deviation for the 5% filled D-60 coatings for both types of silica; the source of this deviation has not yet been determined. The values for A were in agreement with Nielsen's theory predicting higher values of both the Einstein coefficient and the constant A for agglomerated or elongated fillers; agglomerated particles were observed in the sprayed coatings, where the particles were concentrated along the splat boundaries forming a "layered" microstructure. It was believed that in the case of the D-30 coatings the lower values of A were due to an improved spatial distribution of the silica in the polymer matrix than in the D-60 coatings.

Equation (7) was used to estimate the effects of crystallinity increases on the moduli of sprayed

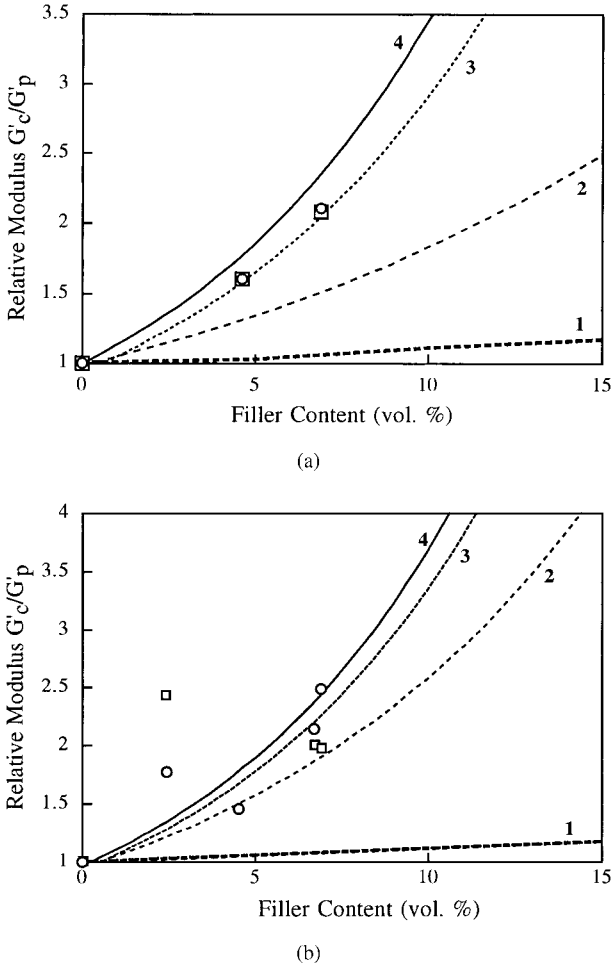

Figure 15 (a) Relative modulus G'_c/G'_p of nylon 11 D-30 coatings at 30°C. Symbols represent experimental values for: (○) hydrophobic silica, (□) hydrophilic silica filler; lines are predictions according to: (1) the rule of mixtures, (2, 3, 4) Kerner's model for A = 2, 3, 4, respectively. (b) Relative modulus G'_c/G'_p of nylon 11 D-60 coatings at 30°C. Symbols represent experimental values for: (○) hydrophobic silica, (□) hydrophilic silica filler, lines are predictions according to: (1) the rule of mixtures, (2, 3, 4) Kerner's model for A = 3, 4, 4.5, respectively.

nanocomposite coatings. The results are illustrated in Figure 16. The increases in moduli of nanocomposite coatings due to crystallinity increases was much higher than those predicted from the model. These estimates strongly indicated that other mechanisms, in addition to variations in crystallinity, were contributing to the reinforcement mechanisms in nanocomposite coatings.

T_g is often reported as the temperature of the maximum loss tangent (tan δ). Values determined in this manner are usually higher than those obtained from G'', because the temperature for $(\tan \delta)_{max}$ is much more sensitive to parameters such as crosslink density, filler content, or blend morphology than T_g itself.[12] The damping peak is associated with the partial loosening of the polymer structure, e.g., breaking of the intermolecular bonds so that groups and small chain segments can move.

Over the 25 to 150°C temperature range studied, one transition was observed for all composite compositions, corresponding to the T_g of the polymer matrix. T_g values, determined from the maximum in the loss modulus G'', are summarized in Table V. The values were similar to those obtained from differential scanning calorimetry analysis. The addition of the reinforcement resulted in a 1–2°C increase in T_g for the D-30 coatings. Hydrophilic and hydrophobic silica filled D-60 coatings exhibited a decrease in T_g with the initial addition of reinforcement. At higher reinforcement contents, however, an increase in T_g of 3–4°C was observed. All silanated silica reinforced coatings exhibited 1–2°C increases in T_g.

Tan δ and its response to the presence of the silica reinforcement are shown in Figure 17(a) and (b) for D-30 and in Figure 18(a) and (b) for D-60 nylon 11 composites. The tan δ peaks at 53 and 58°C corresponded to the maximum damping of the D-60 and D-30 composites, respectively. The addition of nanosized fillers did not cause significant shifting of the damping peak; however, broadening and lowering of the curve peaks with

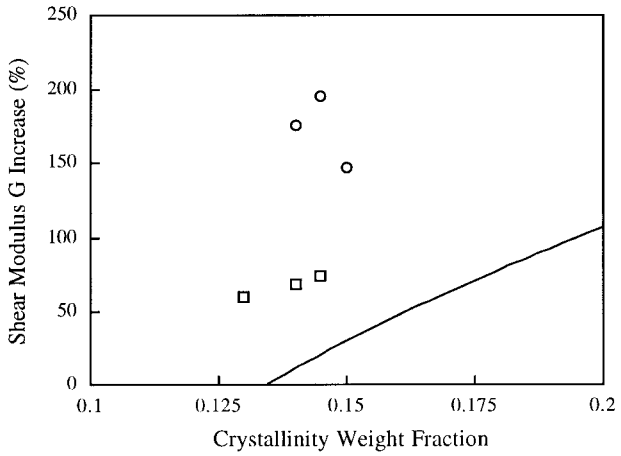

Figure 16 Shear modulus of nanoreinforced coatings as a function of crystallinity content. Experimental data are for: (○) D-60 and (□) D-30 reinforced nylon 11 coatings. The solid line represents the shear modulus prediction according to eq. (7).

Table V Glass Transition Temperatures (T_g) of Thermally Sprayed Nanocomposite Coatings

Silica Content (Nominal Vol %)	Silica Surface Chemistry	Nylon 11 Matrix	T_g (°C)
0	—	D-60	50
0	—	D-30	48
5	Hydrophobic	D-60	46
5	Hydrophilic	D-60	47
5	Silanated	D-60	51
10	Hydrophobic	D-60	48
10	Silanated	D-60	52
10	Hydrophobic	D-30	50
10	Hydrophilic	D-30	50
15	Hydrophobic	D-60	54
15	Hydrophilic	D-60	53
15	Silanated	D-60	52
15	Hydrophobic	D-30	51
15	Hydrophilic	D-30	50

increased reinforcement contents was observed for both silicas in D-30 and D-60 coatings.

In Figure 19 (a) and (b), the damping behavior of the D-30 and D-60 reinforced coatings, respectively, are compared with the predicted non-interactive damping behavior calculated according to Nielsen's model [eqs. (9) and (10)]. According to this theory, deviations from non-interactive behavior suggest the existence of strong polymer-reinforcement interactions and potentially, the formation of immobilized polymer layers in the vicinity of the reinforcement particles. The values of the layer thickness, ΔR, reported in the literature vary, depending on the size and volume fraction of the filler particles and also on the polymer system studied. Kendall and Sherliker[28] reported a 2-nm-thick "bound" polymer layer in polyethylene filled with nanosized silica and carbon black. Similar results for the immobile layer thickness, in the range of 0.5–2 nm, were reported by O'Brien et al.[44] for carbon black in rubber. Iisaka and Shibayama,[29] using eqs. (9) and (10), calculated thicknesses up to 1.4 μm for polystyrene/glass beads (particle radii of 20–60 μm) composites. Using the same model, Boluk and Schreiber[25] calculated the thickness of the immobile layer to be up to 20 nm in chlorinated polyethylene filled with nanosized rutile (TiO_2). The presence of a layer with restricted mobility can result in a decrease in the loss tangent amplitude and a shift in the peak maximum to higher temperatures.

The correction parameter, B, was evaluated from the slope of the tan δ versus ϕ_f plots. The thickness of the "immobilized polymer layer," ΔR, calculated from B values using eq. (10), are summarized in Table VI. The ΔR values, ranging from 3 to 23 nm, appeared to be within the range reported in the literature for various sizes of fillers.[25,27–29,44] ΔR values were lower, 3–7 nm for D-30, compared with 7–11 nm for D-60 coatings, probably again due to differences in the crystallinity content of the two coatings.

Nanosized fillers contributed to crystallization in thermally sprayed nanocomposite coatings as reported previously[11] and therefore it is reasonable to suggest that some increase in crystallinity may be concentrated in the vicinity of the filler

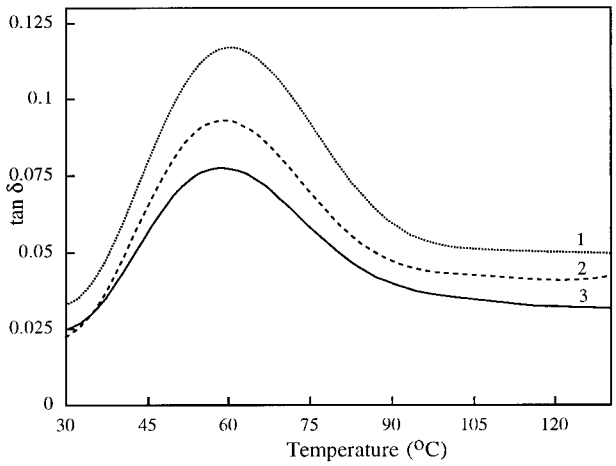

Figure 17 (a) Temperature dependence of tan δ for thermally sprayed nylon 11 D-30 coatings with: (1) 0, (2) 15, and (3) 10 vol % nominal hydrophobic silica content. (b) Temperature dependence of tan δ for thermally sprayed nylon 11 D-30 coatings with: (1) 0, (2) 15, and (3) 10 vol % nominal hydrophilic silica content.

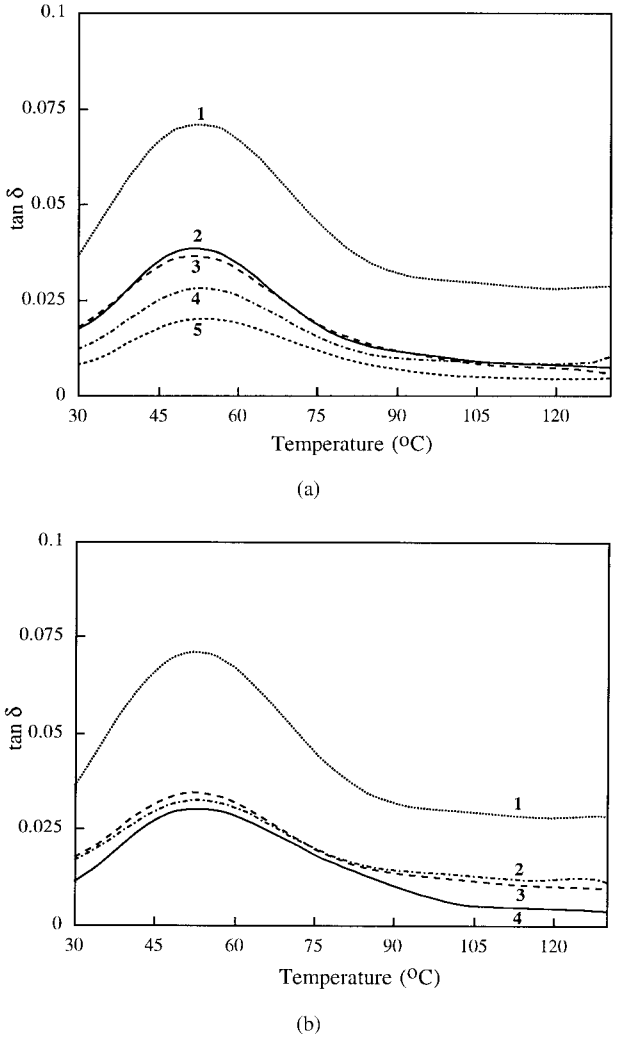

Figure 18 (a) Temperature dependence of tan δ for thermally sprayed nylon 11 D-60 coatings with: (1) 0, (2) 5, (3) 10, (4) 15, and (5) 20 vol % nominal hydrophobic silica content. (b) Temperature dependence of tan δ for thermally sprayed nylon 11 D-60 coatings with: (1) 0, (2) 20, (3) 15, and (4) 5 vol % nominal hydrophilic silica content.

surface. The lamellar spacing of nylon 11 was reported to be between 7–11 nm, depending on the polymer processing and crystallization temperature,[45] consistent with the calculated ΔR values. The morphology of the "immobile" layer in thermally sprayed nanocomposite coatings, however, has not been confirmed at this stage.

Permeability

The results shown in Figure 20 indicated that the water vapor transmission rate (WVTR) through the thermally sprayed nanocomposite coatings decreased with the addition of nanosized silica and carbon black reinforcements. Five percent hydrophobic and 5% hydrophilic silica reinforced D-60 coatings exhibited 16% and 18% decreases in WVTR, respectively, relative to pure D-60 polymer coatings. With increasing reinforcement contents the WVTR decreased further, reaching a maximum of 22.5% for 15% hydrophobic silica reinforced D-60 coatings. Only small differences in WVTR between different types of reinforcements were observed.

More significantly, pure nylon 11 D-30 coatings exhibited substantially lower values (by ~50%) of

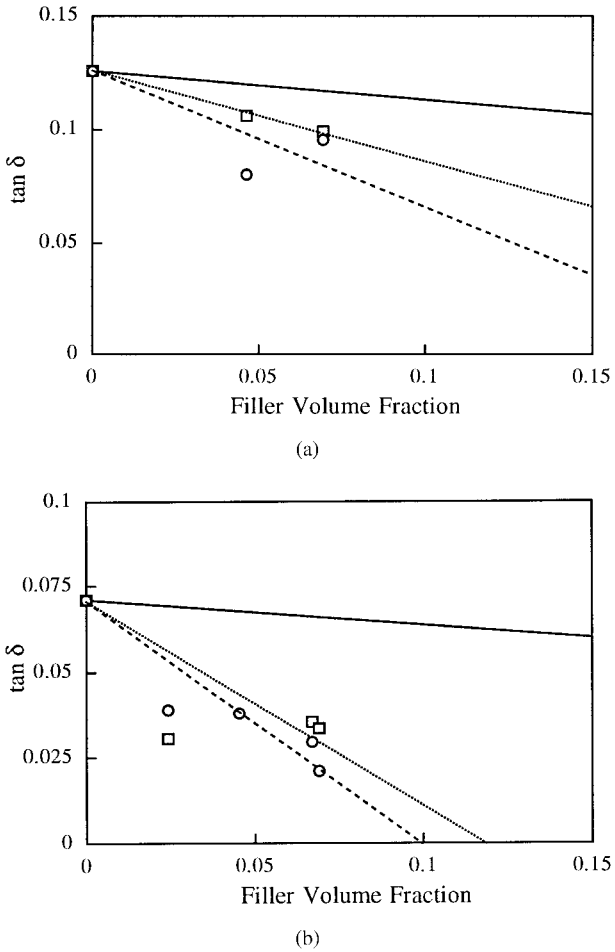

Figure 19 (a) Loss tangent as a function of filler content for nylon 11 D-30 coatings. Experimental data for (○) hydrophobic and (□) hydrophilic silica filler. The solid line is the prediction for rigid, non-interacting fillers [according to eq. (9)]. (b) Loss tangent as a function of filler content for nylon 11 D-60 coatings. Experimental data for (○) hydrophobic and (□) hydrophilic silica filler. The solid line is the prediction for rigid, non-interacting fillers [according to eq. (9)].

Table VI Values of B Parameter and ΔR of Thermally Sprayed Nanocomposite Coatings Calculated According to Eq. (10)

Silica Content (Nominal Vol %)	Silica Surface Chemistry	Polymer Matrix	B	ΔR (nm)
5	Hydrophobic	D-60	18.6	11.5
5	Hydrophilic	D-60	23.5	22.4
5	Silanated	D-60	25.2	13.5
10	Hydrophobic	D-60	10.2	8.2
10	Hydrophobic	D-30	7.8	6.9
10	Hydrophilic	D-30	3.4	6.1
10	Silanated	D-60	13.3	9.6
15	Hydrophobic	D-60	8.7	7.4
15	Hydrophobic	D-30	3.5	3.6
15	Hydrophilic	D-60	7.4	11.4
15	Hydrophilic	D-30	3.1	5.5
15	Silanated	D-60	10.7	8.4

WVTR than pure D-60 coatings. The incorporation of the silica filler in the D-30 coatings resulted in further significant decreases in WVTR. The lowest WVTRs were exhibited by D-30 coatings filled with 10 vol % of hydrophilic silica. Equivalent reductions in WVTR using hydrophobic silica in D-30 coatings required the addition of a nominal 15 vol % content reinforcement.

Permeation of water vapor is believed to occur almost exclusively through the amorphous regions of the polymer; a decrease in diffusion coefficient with increasing crystallinity is usually observed.[30] As expected, aqueous permeability decreased with both increasing crystallinity and reinforcement contents. The improvement was not linear with reinforcement content, showing the greatest changes after the initial addition of reinforcement, and leveling off at higher contents. This appeared to be a result of filler distribution; despite an increase in filler content, a significant volume of the filler remained concentrated in silica rich areas at the splat boundaries,[11] allowing increased diffusion through the polymer-rich areas. The initial addition of the reinforcing phase likely created the silica-rich barriers to vapor diffusion, therefore, such that additional filler had a less pronounced effect on the barrier properties.

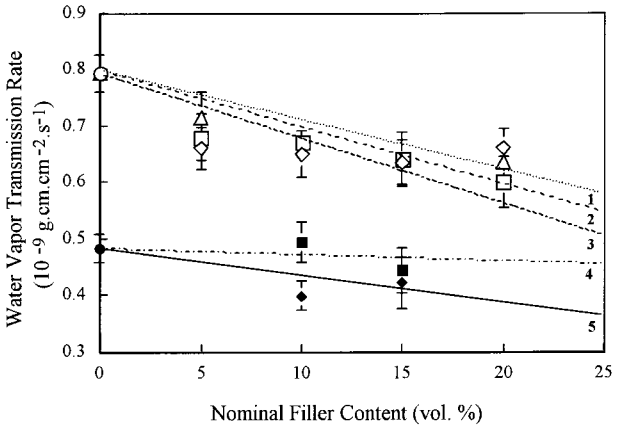

Figure 20 Changes in WVTR of thermally sprayed nanocomposite coatings due to increasing amounts of reinforcement. Legend: unfilled symbols, nylon 11 D-60 composites; filled symbols, nylon 11 D-30 composites: (○) 0% reinforcement, (□, ■, lines 1, 4) hydrophobic silica, (◇, ◆, lines 3, 5) hydrophilic silica, and (△, ▲, line 2) carbon black.

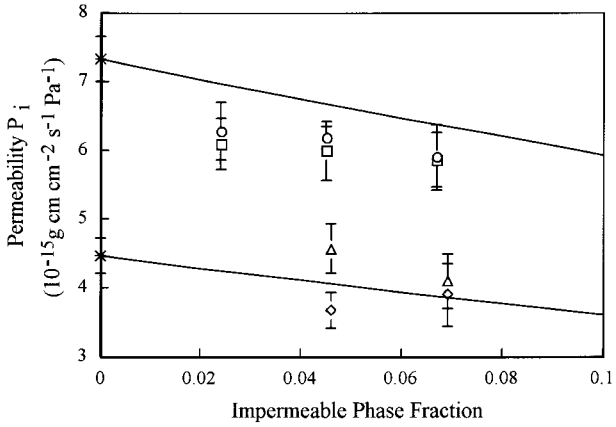

Figure 21 Permeability of nanocomposite coatings as a function of crystalline (impermeable) phase content. Experimental data are for: (○) hydrophobic and (□) hydrophilic silica fillers in D-60 nylon 11; (△) hydrophobic and (◇) hydrophilic silica filler in D-30 nylon 11. Solid lines represent the permeability predicted according to eq. (11).

As shown in Figure 21, the aqueous permeabilities of D-60 nanocomposite coatings were lower than predicted from theory according to eq. (11). Although the theory did not specifically separate the effects of crystallinity and filler, it was clear that the decrease was greater than that predicted for either effect alone, and that both effects likely were contributing simultaneously. The nylon 11 D-30 coatings, however, exhibited lower WVTR than D-60 coatings despite their lower crystallinity content.

As shown in Figure 22, the density of the coatings also appeared to have a significant effect on the coating permeability behavior. Coatings produced from the D-30 powders were always

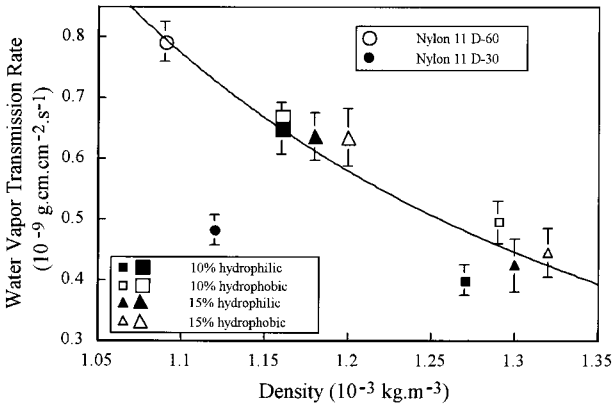

Figure 22 WVTR of thermally sprayed nanocomposite coatings as a function of density. Circle (○), square (□), and triangle (△) symbols represent 0, 10, and 15 vol % nominal filler contents, respectively, in nylon 11 D-30 (smaller symbols) and nylon 11 D-60 (larger symbols). Open symbols (□) and (△) represent hydrophobic silica; closed symbols (■) and (▲) represent hydrophilic silica.

slightly denser than those sprayed from the coarser D-60 powder. The nylon 11 D-30 coatings also exhibited significantly reduced WVTR compared with the D-60 with corresponding filler contents. Nylon 11 D-30 coatings also had slightly lower porosity contents, 0.5–1.5%, compared with 0.7–1.9% for D-60 coatings.[11]

The slightly higher densities of the D-30 coatings were an expected result of the processing conditions: the smaller D-30 particles likely were more homogeneously heated than the larger D-60 particles. The more completely melted D-30 particles filled the underlying interstices more effectively upon splatting, thereby reducing the number and volume of pores created during deposition and increasing the cohesion of the coating. This led to a larger reduction in the WVTR for the D-30 coatings despite the higher crystallinity content of the D-60 coatings. Coating porosity and density therefore seemed to have a dominant influence on the aqueous permeability behavior of HVOF sprayed nanocomposite coatings with semicrystalline structures. Further detailed studies on the coating structure and crystal morphology are currently in progress to evaluate their effect on the coating permeability behavior.

CONCLUSIONS

Nanoreinforced polymer coatings deposited using the HVOF combustion spray process exhibited significantly increased scratch and wear resistance, and improved mechanical and barrier properties over thermally sprayed pure polymer coatings. Higher scratch resistances were measured in coatings produced from the powder with larger polymer particles (D-60), likely due to the higher crystallinity of these coatings. The largest improvements in scratch resistance, 30% and 35%, were exhibited by 15% hydrophobic silica and 15% carbon black reinforced D-60 coatings, respectively. Similarly, the highest wear resistances were measured for 15% hydrophobic silica and for all carbon black reinforced D-60 coatings. The increased wear resistance represented 48% and 67% improvements relative to thermally sprayed pure nylon D-60 coatings.

Increases in crystallinity and reinforcement content both resulted in increases in the glass storage modulus for silica reinforced coatings. A greater increase in dynamic storage modulus than expected from the rule of mixtures was measured for all silica-reinforced coatings. The maximum increase in dynamic storage modulus below the T_g relative to pure nylon 11 D-60 coatings was exhibited by 15% silanated silica D-60 coatings (205%), followed by 15% hydrophobic silica reinforced D-30 coatings (182%). The largest increase in modulus in D-60 coatings was measured for 15% hydrophobic silica coatings (120%). Polymer-reinforcement particle interactions appeared to dominate this improvement in moduli below T_g. Above T_g, D-60 nanocomposite coatings exhibited higher moduli than D-30 coatings due to the higher crystallinity content of the D-60 coatings.

The WVTR of all reinforced coatings were lower than those of pure polymer coatings. The 15% hydrophobic silica reinforced D-60 coatings exhibited a 22.5% decrease in WVTR, reaching a value of 0.63×10^{-9} g cm cm^{-2} s^{-1}. The WVTR of D-30 coatings was even lower, due to the decrease in porosity. The lowest WVTR of 0.39×10^{-9} g cm cm$^{-2\ s-1}$ was exhibited by 10% hydrophilic silica reinforced D-30 coatings, a 50% improvement in WVTR relative to unfilled D-60 coatings.

Crystallinity and reinforcement content seemed to have a dominant effect on the mechanical properties of thermally sprayed coatings, whereas coating density dominated the permeation behavior of nanoreinforced coatings.

This paper is based upon work supported by the National Science Foundation under Grant No. 9713650. The work does not represent the opinion of the National Science Foundation. The authors would like to

thank Elf Atochem North America, Inc. and Degussa Corporation for the donation of powders and Stellite Coatings for donation of the 0.076-m nozzle used for this work. The authors greatly appreciate the assistance by Mr. Don Gentner during thermal spraying and Mr. David von Rohr during SEM analysis.

REFERENCES

1. Sumita, M.; Shizuma, T.; Miyasaka, K.; Ishikawa, K. J Macromol Sci Phys 1983, B22, 601.
2. Sumita, M.; Tsukumo, T.; Miyasaka, K.; Ishikawa, K. J Mater Sci 1983, 18, 1758.
3. Messersmith, P. B.; Giannelis, E. P. Chem Mater 1994, 6, 1719.
4. Messersmith, P. B.; Giannelis, E. P. J Polym Sci A Polym Chem 1995, 33, 1047.
5. Yano, K.; Usuki, A.; Okada, A.; Kurauchi, T.; Kamigaito, O. J Polym Sci Part A Polym Chem 1993, 31, 2493.
6. Lewis, T. B.; Nielsen, L. E. J Appl Polym Sci 1970, 14, 1449.
7. Kumar, V.; Erwin, L. Antec '87, 1987, 152.
8. Giannelis, E. P. Adv Mater 1996, 8, 29.
9. Burnside, S. D.; Giannelis, E. P. Chem Mater 1995, 7, 1597.
10. Schadler, L. S.; Laul, K. O.; Smith, R. W.; Petrovicova, E. J Therm Spray Technol 1997, 6, 475.
11. Petrovicova, E.; Knight, R.; Schadler, L. S.; Twardowski, T. J Appl Polym Sci 2000, 77, 1684.
12. Nielsen, L. E.; Landel, R. F. Mechanical Properties of Polymers and Composites; Marcel Dekker: New York, 1994.
13. Einstein, A. Ann Phys 1906, 19, 289; 1911, 34, 591.
14. Guth, E. J Appl Phys 1945, 16, 20; Smallwood, H. M. J Appl Phys 1944, 15, 758.
15. Sato, Y.; Furukawa, J. Rubber Chem Technol 1962, 35, 857.
16. Mooney, M. J Colloid Sci 1951, 6, 162.
17. Eilers, H.; Van Dyck, L. Kolloid Z 1941, 97, 313.
18. Bills, K.; Sweeny, K.; Salcedo, F. J Appl Polym Sci 1960, 12, 259.
19. Eckstein, Y.; Dreyfuss, P. J Polym Sci Polym Phys 1982, 20, 49.
20. Quemada, D. Rheol Acta 1972, 16, 82.
21. Frankel, N. A.; Acrivos, A. Chem Eng Sci 1967, 22, 847.
22. Kerner, E. H. Proc Phys Soc 1956, B69, 808.
23. Nielsen, L. E. J Polym Sci Polym Phys 1979, 17, 1897.
24. Lewis, T. B.; Nielsen, L. E. Trans Soc Rheol 1968, 12, 421.
25. Boluk, M. Y.; Schreiber, H. P. Polym Compos 1986, 7, 295.
26. Vollenberg, P. H. T.; Heikens, D. Polymer 1989, 30, 1656.
27. Giannelis, E. P. JOM 1992, 44, 28.
28. Kendall, K.; Sherliker, F. R. Br Polym J 1980, 12, 85.
29. Iisaka, K., Shibayama, K. J Appl Polym Sci 1978, 22, 3135.
30. Goosey, M. T. In Polymer Permeability; Comyn, J., Ed.; Elsevier Applied Science: New York, 1985; p. 309.
31. de Candia, F.; Vittoria, V. J Appl Polym Sci 1994, 51, 2103.
32. McCrone, W. C. In Physics and Chemistry of the Organic Solid State; Fox, D.; Labes, M. M.; Weissberger, A., Eds.; John Wiley & Sons: New York, 1965.
33. Eitzman, D. M.; Melkote, R. R.; Cussler, E. L. AIChE J 1996, 42, 2.
34. Cussler, E. L.; Hughes, S. E.; Ward, W.J .; Rutheford, A. J Membr Sci 1988, 38, 161.
35. Barrer, R. M. In Diffusion in Polymers; Crank, J.; Park, G. S., Eds.; Academic Press: London, 1968.
36. Plueddemann, E. P. Silane Coupling Agents; Plenum Press: New York, 1982.
37. Annual Book of ASTM Standards, D-5178-91; ASTM: Philadelphia, 1991; Vol. 06.01.
38. Annual Book of ASTM Standards, D-1653-93; ASTM: Philadelphia, 1991; Vol. 06.01.
39. Miller, E. Introduction to Plastics and Composites; Marcel Dekker: New York, 1996.
40. Perkins, W. G.; Porter, R. S. J Mater Sci 1981, 16, 1458.
41. Buckley, D. H. Friction, Wear and Lubrication in Vacuum, Scientific and Technical Information Office; National Aeronautic and Space Administration: Washington, D.C., 1971.
42. Ramasubramanian, N.; Krishnamurthy, R.; Malhotra, S. K. Wear 1993, 163-164, 631.
43. Clerico, M. Wear 1969, 13, 183.
44. O'Brien, J.; Cashell, E.; Wardell, G. E.; McBriety, V. J. Macromolecules 1976, 9, 653.
45. Dosiere, M.; Point, J. J. J Polym Sci Polym Phys 1984, 22, 1383.